Computational Differentiation of Bronsted Acidity Induced by Alkaline Earth or Rare Earth Cations in Zeolites

ARTICLE *in* INORGANIC CHEMISTRY · NOVEMBER 2012

Impact Factor: 4.76 · DOI: 10.1021/ic301279v · Source: PubMed

3 AUTHORS:

Andrey A. Rybakov
Lomonosov Moscow State University
17 PUBLICATIONS **44** CITATIONS
SEE PROFILE

Alexander Larin
Lomonosov Moscow State University
68 PUBLICATIONS **369** CITATIONS
SEE PROFILE

Georgy Zhidomirov
Russian Academy of Sciences
402 PUBLICATIONS **2,669** CITATIONS
SEE PROFILE

Inorganic Chemistry

Article

pubs.acs.org/IC

Computational Differentiation of Brønsted Acidity Induced by Alkaline Earth or Rare Earth Cations in Zeolites

Andrey A. Rybakov,*[,†] Alexander V. Larin,[†] and Georgy M. Zhidomirov[†,‡]

[†]Chemistry Department, Lomonosov Moscow State University, Leninskiye Gory 1-3, GSP-1, Moscow 119991, Russia

[‡]Boreskov Institute of Catalysis, Siberian Branch of the Russian Academy of Sciences, Pr. Akad. Lavrentieva 5, Novosibirsk 630090, Russia

Supporting Information

ABSTRACT: For bi- and trivalent Me^{q+} (Me = metal) cations of alkaline earth (AE) and rare earth (RE) metals, respectively, the formation of the nonacid $MeOH^{(q-1)+}$ species and acid H−O_{zeo} group, where O_{zeo} is the framework atom, from water adsorbed at the multivalent $Me^{q+}(H_2O)$ cation in cationic form zeolites was checked at both isolated cluster (8R or 6R + 4R) and periodic (the mordenite framework) levels. Both approaches demonstrate qualitative differences for the stability of the dissociated water between the two classes of industrial cationic forms if two Al atoms are closely located. The RE forms split water while the AE ones do not, that can be a basis of different proton transfer in the RE zeolites (thermodynamic control) than in the AE forms (kinetic control). The cluster models allow quantitatively explaining nearly equal intensities $I_{HF} \sim I_{LF}$ of the high frequency (HF) and low frequency (LF) OH vibrations in the RE forms and lowered $I_{HF} \ll I_{LF}$ in the AE forms, where HF bands are assigned to the Me−OH groups in the RE and AE forms, respectively, while LF bands are assigned to the Si−O(H)−Al groups. The role of electrostatic terms for water dissociation in the RE and AE forms is discussed.

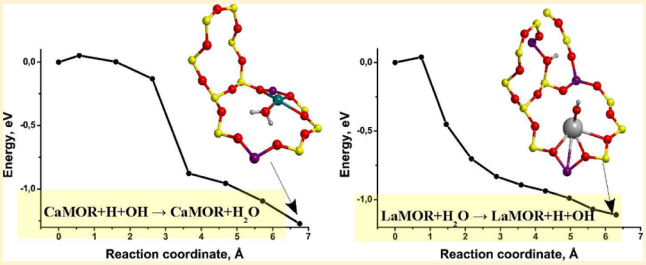

INTRODUCTION

The Brønsted acidity of both of alkaline earth and rare earth cationic form zeolites is well-known.[1] The usual explanation suggests water dissociation at 2- or 3-valent cations, respectively. However, few pieces of theoretical and experimental evidence have been collected. The experimentalists mainly appeal to the presence of hydroxyl peaks in the spectra, leaving the hydroxyl formation mechanism unknown. The authors of ref 2 were unable to find any structure corresponding to heterolytic dissociation of water

$$Me^{q+}(H_2O) + (Si - O - Al)^- \rightarrow MeOH^{(q-1)+} + Si - O(H) - Al \quad (1)$$

for Me = Zn (q = 2) over six-member (6R) window of the ZnY type. In contrast to the Y zeolite fragments the structures corresponding to water heterolytic dissociation on Zn^{2+} in various 5R zeolite cycles were found.[2] The process 1 was calculated as exothermic (21.6−28.1 kcal/mol in three 5R windows cut from ZnZSM-5). The calculated energy of molecular adsorption over the 6R window of ZnY was found to be quite significant (29 kcal/mol),[2] but no comparison of the energies of molecular and dissociative adsorption for the same 5R clusters was given in this work. We would note that the energy of molecular adsorption (29 kcal/mol)[2] is close to our results obtained for CaMOR (MOR = mordenit) at the periodic level (see Table 3 in ref 3). In the article[4] for Zn^{2+} in 5R zeolite cycle and in α-position of ZSM-5, it was found that for these cluster models molecular adsorption (specifically, $Zn(H_2O)^{2+}$ formation) is more stable (on 11.94 kcal/mol) than dissociative one (eq 1). Hence, the theoretical justification of reaction 1 for any zeotype and any cation remains uncertain.

Later on, the authors of the current work have found that divalent AE cations cannot split water if two Al atoms are located close enough one to another near the cationic site.[3] Only remote pairs of Al atoms can thus produce stabilized hydroxyl groups. The main reason to trap the hydroxyls is the barrier between the current proton location near remote Al and the one that is more energetically reasonable. In such a way, the trapping of the hydroxyl groups has a kinetic nature of the OH stabilization rather than thermodynamic one (owing to the large difference in the deprotonation energies).

In this work, water dissociation is discussed in the La cationic forms that possess a higher electric field relative to that of the AE ones. The spectroscopic evidence[5−7] supports OH formation in the RE forms with some differences between various RE cations (La, Ce, ...) (Table 1). Additional proof in favor of eq 1 comes from X-ray[8,9] and neutron[8] diffraction analyses in LaY with the different number of water molecules coordinated to $La^{3+}(H_2O)_m$ cation ($1 < m < 2$) and completely dissociated. Both cluster and periodic approaches are applied to study this reaction 1 using Me = La (q = 3) for a first time to our best knowledge. After the presentation of technical details,

Received: June 17, 2012

dx.doi.org/10.1021/ic301279v | Inorg. Chem. XXXX, XXX, XXX−XXX

Table 1. Experimental Spectra (cm^{-1}) of RE Form MeY Zeolites (Me = La, Ce)

type	LaY (5)	CeY (5)	CeY (6)	CeY (7)[a]	CeY (7)[b]
silanol	3745	3745	3750	3740	3740
Me−OH	3685	3685			
Me−OH	3645	3650	3640	3630	3640
Me−OH?				3618	
Si−OH−Al	3520	3535	3555	3555	3522

[a]At 230 °C. [b]At 460 °C.

the results for the AE and RE forms are obtained and compared. The electrostatic nature of water dissociation in the RE and AE forms is finally discussed. Electrostatic field (EF) values that are required to justify the electrostatic character are compared to the experimental data.

COMPUTATIONAL DETAILS

The isolated cluster approach was performed using GAUSSIAN03[10] at the B3LYP and MP2 levels and GAUSSIAN09[11] at the B97D and M06L levels using 6-31G*(Si, Al, O, H, Ca)/LANL2DZ(La) basis set. Two types of the clusters have been used. The first is the 8-member ring (8R) of MOR, and the second is the Y zeolite fragment that includes two 6R and 4R windows (6R + 4R) having one common Si−O−Si moiety. More technical details about the cluster models are presented in refs 12−14.

At the periodic level, we optimized reactant and product geometries for the reaction between H_2O and Me cations, Me = Ca and La, in the mordenite (MOR) zeolite with different distances between Al atoms using the VASP 5.2 code.[15] The projected-augmented wave (PAW) method[16] and the gradient-corrected PBE functional[17] were used. The PW91 functional[18] was also tested, and it gave similar results (Tables 2 and 6). The energy cutoff was set to 500 eV. The Brillouin zone sampling was restricted to the Γ-point. For calculating the minimum energy path between reagents and products, we used the climbing image nudged elastic band (NEB) method.[19] Vibrational frequencies were calculated using the finite difference method as implemented in VASP. Small displacements (0.015 Å) of the atoms from the H_2O species were used to estimate the numerical Hessian matrix. The rest of the zeolite atoms were kept fixed at their equilibrium positions. Visualization at both cluster and periodic levels was realized with the MOLDRAW code.[20]

For Me = La we started from the same Al positions that have been constructed in the CaMOR zeolite[3] and replaced one additional Si by Al for neutrality. So, the models contain two Al atoms in the 8R ring and one Al atom in (a) opposite 8R ring in the main channel (models 2, 2a), (b) the nearest connected 6R ring of the main channel (models 1, 1a, 3, 3a), or two Al atoms in two 8R opposite rings and one Al atom in the nearest connected 6R ring (model 4).[3] The protons are trapped in the opposite 8R ring (model 2), in the nearest connected 6R ring (models 1, 3, 4), or in the 8R ring (models 1a, 2a, 3a). The models 1a, 2a, and 3a have been obtained from 1, 2, and 3 by proton displacement from the wall to the 8R window.

For analysis of electron density, atomic multipole moments up to hexadecapoles (all the atoms) or dipoles (H atoms) have been calculated using the GDMA 2.0 code.[21] Respective calculations with GDMA have been started from formatted *chk* file after using GAUSSIAN03 code for cluster models.

Table 2. Energies (eV) of the CaMOR Cell (E_{cell}) Together with Adsorbed Water ($E_{cell+H2O}$) or with the Dissociation Products ($E_{cell+OH+H}$), and the Energy of Water Adsorption ($\Delta U_{H2O} = E_{cell+H2O} - E_{cell} - E_{H2O}$)[a]

site	E_{cell}	$E_{cell+H2O}$	ΔU_{H2O}	$E_{cell+H+OH}$
		PBE		
A	−1141.11	−1156.33	−0.95	n/o
C	−1138.52	−1153.03	−0.24	n/o
D1	−1139.73	−1155.57	−1.57	n/o
D2	−1140.05	−1155.66	−1.34	n/o
D3	−1139.27	−1155.05	−1.51	−1154.05
		PW91		
A	−1149.06	−1164.37	−1.04	n/o
C	−1146.49	−1160.97	−0.21	n/o
D1	−1147.68	−1163.62	−1.67	n/o
D2	−1148.02	−1163.72	−1.43	n/o
D3	−1147.24	−1163.37	−1.58	−1162.12
		−1162.20[b]	−1.09	−1161.11[b]
		−1162.48[c]	−1.28	−1161.20[c]

[a]All calculations were performed with the VASP 5.2 code at the PBE and PW91 levels. The total energy of water molecule is E_{H2O} = −14.27 eV for PBE and E_{H2O} = −14.21 eV for PW91. No dissociation products were obtained (n/o) at the sites A, C, D1, and D2. [b]Upon fixed framework atoms and mobile H and OH atoms. [c]Upon fixed framework atoms and mobile Ca, H, and OH atoms.

RESULTS

AE Forms. In the case of AE forms the cluster models have been earlier studied[3] so that only the periodic models are given herein. For the AE cations we checked all possible sites with various local geometries that could influence on the hydroxyl stability.[22] Some heats of water adsorption for the AE centers have been mentioned in ref 3 while the detailed analysis of respective centers is presented below for the CaMOR models (Table 2 and Figure 1). In order to resolve the question about water dissociation in AE forms we tested the possible cationic sites assigned on the basis of the CO adsorption in MgMOR.[22] Their clear hierarchy determines the convenience of this classification in the terms of electric field (EF) as it was demonstrated,[21] because EF could be one of the main factors that stimulate the dissociation.

At first, we have optimized the MgMOR models approved by ref 22 but by replacing the Mg cations by Ca ones (Figure 1) located at sites A (side channel with strongly compressed eight-membered rings parallel to the main channel), C (non planar six-ring in two bent five-rings), D1, and D2 (both in eight-member ring in the main channel with Al−Si−Al and Al−Si−Si−Al alternations in the rings, respectively). After that we have added H_2O near to Ca cation and tried to optimize the products of water dissociation. The energies of corresponding models are given in Table 2. The CO spectra correspond to the highest occupation by Mg of the A and C centers[22] that undoubtedly possess lower electric field as compared to the D and E sites with higher electric field. The shift for CO is mainly determined by the dipole component being proportional to electric field value in Na form zeolites (Table 4 in ref 23) and hence in Ca forms as well due to the higher cationic charge and electric field. We remind the reader that we considered water dissociation at the D3 site (also as model 0 in ref 3) of CaMOR being one of two D and E centers with highest interaction energies and shifts shown in ref 22. It signifies that the same reaction over Ca cation at the A or C sites could hardly result in water dissociation due to a weaker field. Indeed, we did not succeed in modeling the water cleavage at both A and C sites.

In agreement with the observations in ref 5 for preferred adsorption of CO in MgMOR, site A is also the favored one for H_2O in CaMOR (−1141.11 eV in the second column in Table 2 and Figure 1a). On the opposite, site C is much less attractive for H_2O (Figure 1b). More precisely, the sequence A < D2 < D1 < D3 < C corresponding to the deepest A site is obtained.

dx.doi.org/10.1021/ic301279v | Inorg. Chem. XXXX, XXX, XXX−XXX

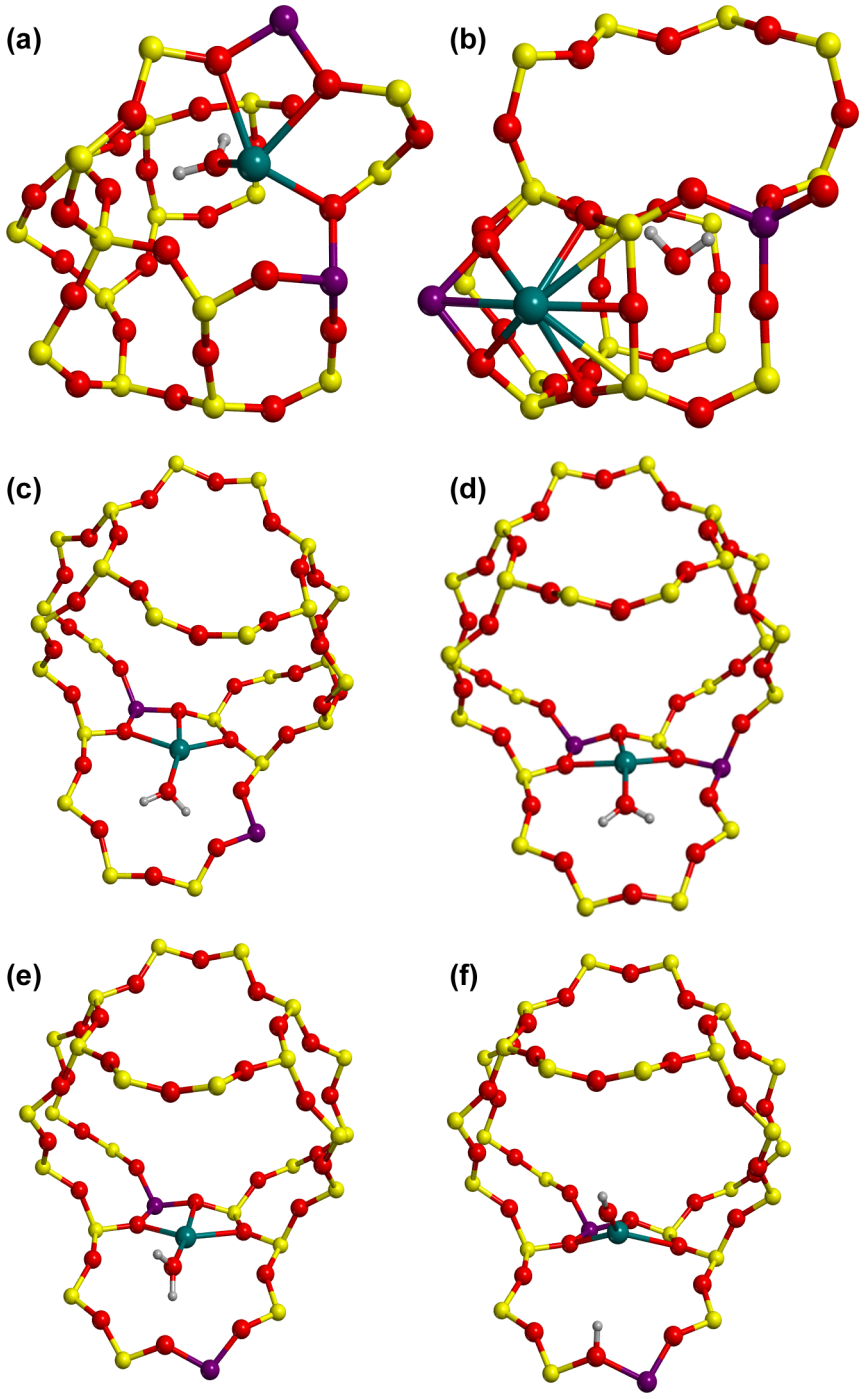

Figure 1. Geometries for water location in CaMOR with the different positions of Al atoms (a−e), products of water dissociation (f) calculated at the PBE level. The models A (a), C (b), D1 (c), D2 (d), and D3 (e, f) are shown. The color code: O in red, Si in yellow, Al in violet, Ca in cyan, H in gray (small spheres).

So, at small coverage the energy of adsorption ΔU should be close to the 0.95 eV (site A) or 21.91 kcal/mol (Table 2). Considering the slight decrease of the zero point energy (ZPE) (methods of ZPE correction calculations are given in the ref 3) upon adsorption we obtained the heat of adsorption of 21.77 kcal/mol at site A. The higher heats of water adsorption correspond to the sites with the lower occupations such as the D1 (36.66 kcal/mol), D3 (35.05 kcal/mol), D2 (31.08 kcal/mol) sites. Nevertheless, the heats averaged over all the A, D2, and so forth centers should be close to the experimental data of 30.5 and 27.9 kcal/mol at 293 and 468 K, respectively,[24] being higher than 23.2−12.2 kcal/mol from other sources.[25,26] The same trends are shown at the PW91-GGA level regarding relative occupations and heats of adsorption (lower part of Table 2). The relative energies at different sites also become closer after water adsorption. In sites D1 and D2 the proton is located too close to the OH group, resulting in an unstable configuration where H_2O easily recombines. In the site D3 the distance between Al atoms in 8R ring is maximal (8.31 Å), thus making possible the existence of the stable CaOH + H(MOR) configuration. Indeed, we observed a preferred water recombination with the minor barrier of 1.20 kcal/mol with

dx.doi.org/10.1021/ic301279v | *Inorg. Chem.* XXXX, XXX, XXX−XXX

the reaction coordinate corresponding to the HO−Ca···OH angle and small imaginary frequency of 34.2i cm^{-1}. Namely, this angular dependence is the reason for the small imaginary frequency for the transition state (TS) illustrated by animation file in the Supporting Information of ref 3. One has to note nearly immobile Ca position along the reaction coordinate. It is the main reason for the conservation of the exothermic character of water recombination, i.e., the heat is −1.09 instead of −1.58 kcal/mol (model D3 in Table 2), if the reaction is modeled at the fixed framework atoms and only mobile H and O atoms of water and OH group.

In order to guess the origin of similar small barrier (1.44 kcal/mol at the B3LYP/6-31G* level [3]) in the Mg(6R + 4R) cluster we have checked the other DFT functionals such as B97D with improved dispersive energy[28] and local meta-GGA M06L one[29] (Table 3). The largest fall of the barrier up to 0.26 kcal/mol in the recombination has been obtained for B97D, while deleting the Hartree−Fock exchange part led to a slight growth of the barrier (1.92 kcal/mol). We consider these results as a confirmation of the stability of water versus dissociation at the cationic positions near two closely positioned framework Al atoms in CaMOR. The agreement with experimental heats of adsorption shows the absence of overstabilized adsorbed water in the AE zeolites.

Table 3. Heats (ΔU, kcal/mol), Activation Energies ($\Delta E^{\ddagger}$, kcal/mol), and Imaginary Frequencies (ω, cm^{-1}) for Transition State of Water Recombination Reaction in Mg(6R + 4R) Cluster

value	B3LYP	B97D	M06L
ΔU	8.40	8.29	9.88
$\Delta E^{\ddagger}$	1.44	0.26	1.92
$-i\omega$	834.0	457.2	976.6

RE Forms. Isolated Cluster DFT and MP2 Approaches. For the RE forms the task of this work looks to be simpler than for the AE forms because the dissociation phenomenon is enough to be proven at any site of periodic LaMOR model. In the case of La forms we studied here two 8R and 6R + 4R cluster models,[12−14] which demonstrated similar trends. If water dissociates without barrier in 6R + 4R (Figure 2a), the energy gain for dissociated forms (Figure 2c−e) in the 8R cluster varies with proton position in the 8-ring (Table 4). At shorter H−O···La distances the dissociation can be even forbidden (Figure 2c,d). The latter has an easy explanation due to the OH orientation which cannot satisfy simultaneously the favored linear ion La···O−H dipole position and usually small deviation angle (β) of the hydroxyl relative to the Si−Oz−Al plane, where index z is related to zeolite oxygen (Table 4). This β angle of 34.71° at the B3LYP level and 39.17° at the MP2 level (Table 4) in the less stable dissociation form 8R (Figure 2c) has to be compared with the respectively small values in periodic H-models[27] or in LaMOR models below (Table 5). However, even at such strained OH position the La···Oz-H angle is 106.14° while the La−O−H angle is 173.13° for the hydroxyl subjected to the higher EF. For the stable dissociation form in 8R the OH group orientation aligns better relative to the La field up to 120.76°.

Another important advantage of the dissociation model (Figure 2e) in La8R is related to the explanation of the experimental intensity ratio $I_{HF}/I_{LF} \sim 1$ between the high frequency (HF)/low frequency (LF) OH vibrations of the

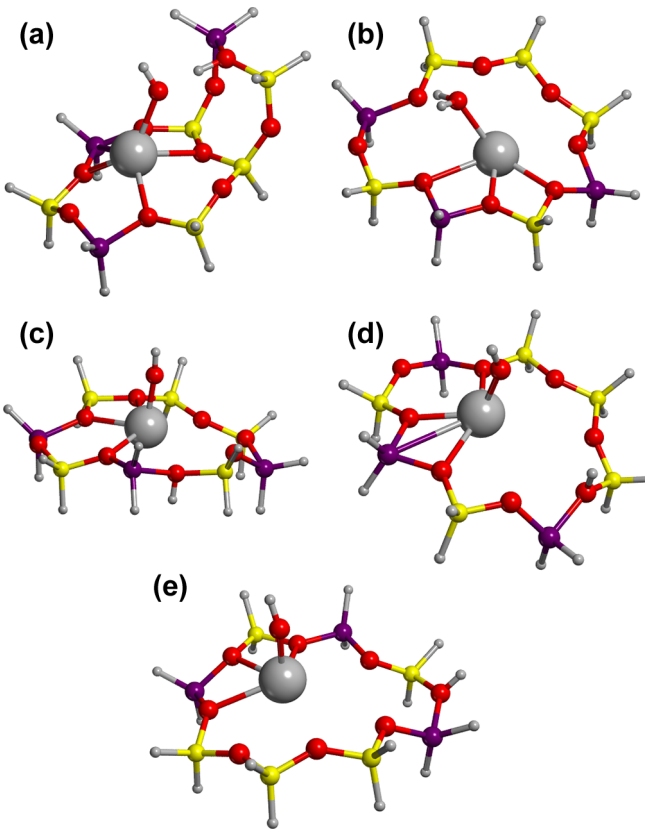

Figure 2. Products of water dissociation (a, c, d, e) and water location (b) in the La(6R + 4R) (a) and La(8R) (b, c, d, e) clusters calculated at the B3LYP/6-31G*(Si, Al, O, H)/LANL2DZ(La) level. The color code is given in Figure1, La in gray (large spheres).

Table 4. Relative Energies $\Delta U = E_{cluster+H+OH} - E_{cluster+H2O}$ (kcal/mol, 23.05 kcal/mol = 1 eV) of the Dissociation Products (the H positions are shown in Figure 2c−e) Compared to That of La(H_2O)8R Model (Figure 2b, Energy Taken as Zero), the Distance R (Å) between O Atom of Si−O(H)−Al Group and La Atom, Deviation Angle β (deg) of the OH Group (Not Linked to La) Relative to the Si−O−Al Plane, La···O−H Angle (Degrees) with Acid OH Group, Intensity Ratio I_{HF}/I_{LF} between the High Frequency (HF)/Low Frequency (LF) OH Vibrations Related to La−OH and Si−O(H)−Al Groups, Respectively, Calculated with B3LYP and MP2 Using 6-31G* Basis Set

R	β	La···O−H	I_{HF}/I_{LF}	Figure	ΔU
		B3LYP Method			
5.306	13.42	120.76	1.0	2e	−15.65
4.271	5.91	84.03	1.2	2d	4.69
3.099	37.71	106.14	2.5	2c	17.26
		MP2 Method			
5.312	14.43	120.62	1.2		−13.96
4.159	3.83	75.54	1.5		7.87
3.065	39.17	107.62	2.9		20.49

peaks at 3640 and 3530 cm^{-1} observed in the CeY spectra (Table 1[6,7]). [The data in ref 7 relate to a mixture of the RE cations in the Y form with the domination of Ce (47%) relative to La (24%), Nd (18%), etc.]

The data for LaY have been presented without intensities in the ref 5, but the band positions are very similar to that in CeY and this I_{HF}/I_{LF} ratio seems to be qualitatively the same for LaY

dx.doi.org/10.1021/ic301279v | Inorg. Chem. XXXX, XXX, XXX−XXX

Table 5. Absolute Energies (eV, 1 eV = 23.05 kcal/mol) of the La(H_2O)MOR ($E_{cell+H2O}$) and LaOH(HMOR) ($E_{cell+H+OH}$) Configurations and Energy Differences $\Delta U = E_{cell+H+OH} - E_{cell+H2O}$ (eV) and Deviation Angle β (deg) of the OH Group (Not Linked to La) Relative to the Si−O−Al Plane for Seven MOR Models (All Al Positions Are Given in Figure 1) with Three Substituted Si/Al Atoms Calculated at the PBE Level

type	Figure	$E_{cell+H2O}$	$E_{cell+H+OH}$	ΔU	β
1	3a	−1155.18	−1156.38	−1.20	8.21
1a	3b		−1156.39	−1.21	10.87
2	3c	−1155.52	−1156.61	−1.08	7.51
		−1154.03[a]	−1154.97[a]	−0.94	
		−1154.12[b]	−11155.11[b]	−1.01	
2a	3d		−1156.59	−1.07	7.42
3	3e	−1155.64	−1156.76	−1.12	17.67
3a	3f		−1156.42	−0.78	8.74
4	3g	−1155.20	−1156.81	−1.61	6.36

[a]Upon fixed framework atoms and mobile H and OH atoms. [b]Upon fixed framework atoms and mobile La, H, and OH atoms.

as well. Also, regarding the small difference of 0.022 Å between covalent or ionic radii of La and Ce atoms at 6-coordinated position (it becomes smaller at higher 8-coordination), one could propose a close similarity between their spectra.[30] The peak positions are qualitatively similar among different works[5−7] and between LaY[5] and CeY[5−7] and remain in the spectra with some drift even at 460 °C.[6,7] If one suggests that the bands at 3645 and 3520 cm^{-1} correspond to the OH bands in the La−OH and Si−OH−Al species, respectively,[5] then our results show on their comparable intensities. More precisely, the intensity ratio I_{HF}/I_{LF} = 1 calculated in La8R between the high frequency (HF)/low frequency (LF) OH vibrations in the La−OH (ν_{HF} = 3836.5 cm^{-1}) and Si−OH−Al (ν_{LF} = 3757.3 cm^{-1}) positions coincides or is very close to the experimental ratio[6,7] (Table 4). Such an intensity ratio I_{HF}/I_{LF} in the AE spectra[7] is usually very small due to smaller intensity of the HF band for Me−OH_2, Me = Mg, Ca, Sr. The energies relative to that of water adsorbed at La cation are pretty similar with both B3LYP and MP2 levels (Table 4). The geometries calculated at the MP2 level are omitted for shortness in Figure 2.

The possibility of hydroxyl stabilization owing to the strong hydrogen bonding (HB) is illustrated via hydrolysis in the 6R + 4R cluster (Figure 2a). Probably, overestimated stabilization as seen from strong red shift, i.e., the La−OH (ν_{HF} = 3777.5 cm^{-1}) and Si−OH−Al (ν_{LF} = 2311.6 cm^{-1}), and intensity ratio I_{HF}/I_{LF} = 23.3 lower the interest to this dissociation model. The experimental I_{HF}/I_{LF} value is usually close to 1 or smaller for RE forms[6,7] while the LF branch is very moderately shifted to the red compared to this La(6R + 4R) case.

The accurate evaluation of the heats of water adsorption or dissociation with the cluster approach is more complex than using the periodic conditions owing to the coupling between the zeolite cluster modes and that of water at smaller frequencies. They are discussed in part S1 in Supporting Information comparing all the zero point energy terms in adsorbed state. Resuming this discussion, we would estimate the error of calculated heats of water adsorption (Table 6) to be less than or equal to 1 kcal/mol.

RE Forms. Periodic DFT Approach. Compared to the 8R cluster model for which the dissociated form can have higher energy (Figure 2c,d) at close Si−O(H)−Al location relative to La (Table 4), the periodic approach demonstrates the possibility of water dissociation for all considered MOR models (Table 5 and Figure 3). The geometry parameters of all the

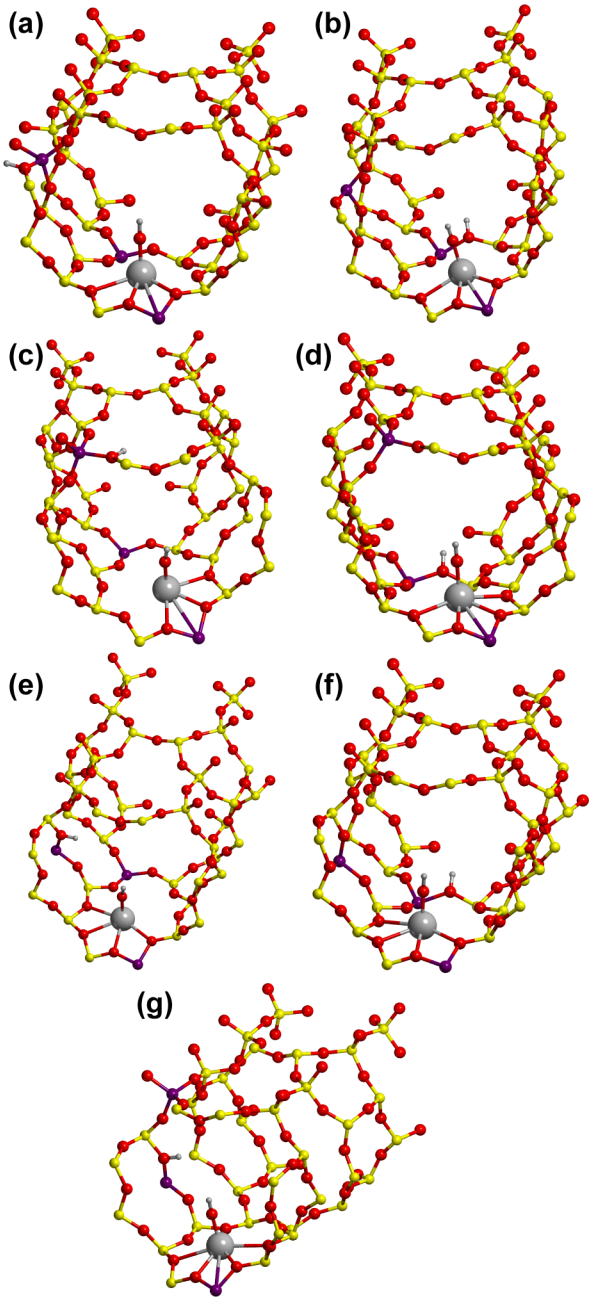

Figure 3. Optimized geometries for the products of water dissociation in LaMOR calculated at the PBE level. The models 1 (a), 1a (b), 2 (c), 2a (d), 3 (e), 3a (f), and 4 (g) are shown. The color code is given in Figures 1 and 2.

models are shown in Table S6. The search of the TS is easier within shorter lAl···All range which corresponds to the smaller distance between the final hydroxyl position and initial water position. For the water dissociation in model 3 that has minimal lAl···All distance (lAl···All for considered models varies between 5.15 and 11.98 Å) we have succeeded in calculating the small barrier of 0.039 eV = 0.89 kcal/mol of water dissociation with the imaginary frequency of 459.1*i* cm^{-1} (Figure 4). The TS is achieved in the course of complex coordinate along the coupled

dx.doi.org/10.1021/ic301279v | Inorg. Chem. XXXX, XXX, XXX−XXX

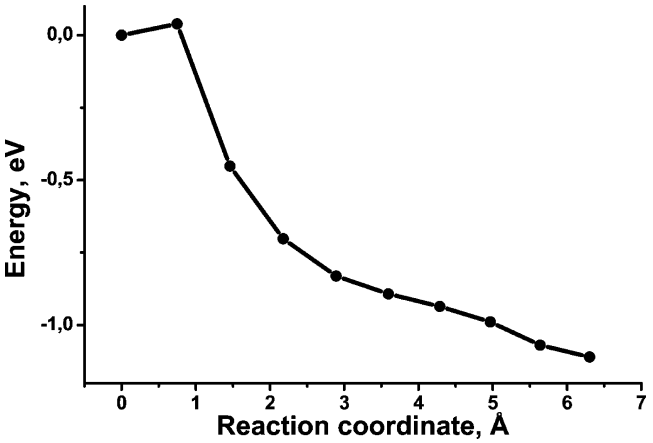

Figure 4. Energy profile of water dissociation along the reaction coordinate in LaMOR (model 3), calculated at the PBE level. The angles and distances at the points 0, 1, and 9 are shown in Table S4.

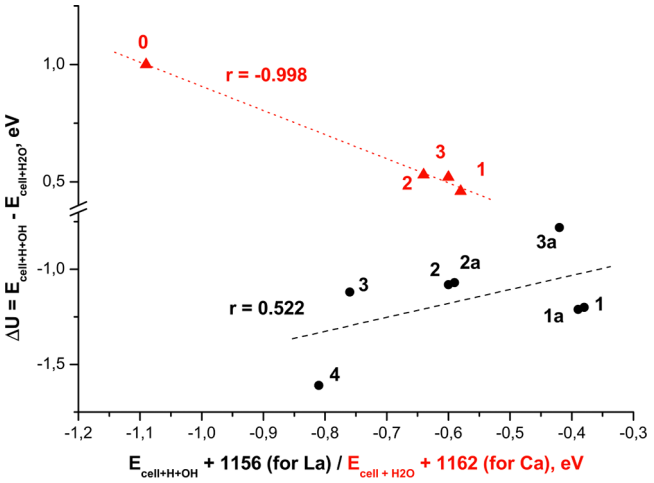

Figure 5. Heat of water dissociation $\Delta U = E_{cell+H+OH} - E_{cell+H2O}$ relative to the heat of water adsorption at the CaMOR (triangles, the models with remote Al positions (3), PW91) and relative to the total energy of dissociated water in LaMOR (circles, models from Table 5, PBE). Correlation coefficients are shown near approximated lines. Respective points are taken from Table 5 and ref 3 (different notations for the energies are used in Table 4 of ref 3).

O···H−O coordinate and the motion of the center of mass of La−O−H species parallel to the 8R plane (please see animation file in the Supporting Information). This value is even smaller than the barrier of 1.20 kcal/mol calculated for water recombination in CaMOR.[3] Despite the La migration parallel to the 8R ring of MOR during the reaction, the restricted optimization of the reagents or products does not change the conclusion about the exothermic water dissociation in fixed framework if either only the O and H atoms are mobile, or the La, O, and H ones (Table 5).

The most favored location of the dissociation products was obtained with model 4 for which the proton is not located near the 8R plane (Table 5). We think that this is due to the distant enough position relative to the La cation for which any alignment of the acidic OH group does not result in essential energy loss in the weaker electric La field. Good agreement of calculated distances between La and framework O atoms, i.e., 2.431, 2.482, 2.801, and 2.862 Å (the model 4), can be noted relative to that determined experimentally via XRD, i.e., from 2.411 to 2.937 Å[8] or from 2.56 to 2.94 Å[9] at room temperature.

We evaluate the critical minimum distance that should be larger than 8−9 Å between the AE cation and oxygen atom of hydroxyl to stabilize the dissociation products. Even if formally such remote position of acid OH group is not required for the RE forms the case of La8R cluster shows that a H sitting too close to La can be questionable because of energy losses owing to the restricted orientation of the OH dipole relative to La field. Such limit can be overcome at the distances that are longer than 5 Å, but exact length depends on the geometry of the site.

The difference between the energies of water dissociation in the AE and RE forms is illustrated in Figure 5. The heat of endothermic dissociation ($\Delta U > 0$) in the CaMOR models depends on the heat of water adsorption while the energies of dissociated forms remain very close in energy, i.e., from −1162.08 to −1162.12 eV for all four models 1−4 (Table 4 in ref 3). The exothermic dissociation ($\Delta U < 0$) in the LaMOR models depends linearly on the stabilization energy of dissociated forms (Figure 5). The accuracy of the ΔU values and the heats of water adsorption ΔU_{H2O} presented in Tables 5 and 6, respectively, are discussed in more details in part S1 and Table S2 in the Supporing Information regarding all ZPE contributions.

This difference between endo- and exothermic dissociation in the AE and RE forms, respectively, allows for justifying the idea of thermodynamic control (due to deprotonation energy variations) and kinetic control for proton locations in the RE zeolites. Only the barrier for proton jumps blocks the H + OH recombination in the AE forms (kinetic control). The calculated and experimental data on the deprotonation energy (DE) or proton affinity (PA) with inverse sign and barriers of the proton jump are compared in Table S7. (Even if the most of the data have been obtained for H-forms they are relevant for our case due to the remote cationic position versus acidic proton.) We can conclude from there that the variations of the DE values between the sites in the studied systems are of the same order of value as the barriers of the proton jump in the same structure (FAU). The different control of proton transfer between active sites in AE and RE form zeolites is extremely important for these two classes of industrial acid catalysts, thus showing that upon raising temperature their respective changes of the catalyst Brønsted acidity are obeyed to different factors in the AE and RE forms. At high temperature (>673 K) of catalytic cracking no new acidic sites are formed in the USY zeolite from water,[31] so that the acidity will be determined by hydroxyls already formed at lower temperatures. Then the Brønsted acidity will be more stable at higher temperatures in the RE forms than in the AE forms. If a proton can reach the area around AE cation with higher temperature, then it can recombine with OH group thus lowering acidity of the AE forms. The expansion of such analysis to other zeolites is required in the future.

Another relevant similarity with the USY zeolites[31] is the presence of the extra framework Al (EFAL) species which are usually discussed as the reasons for enhanced USY acidity after dealumination. Detailed experimental[32−35] and computational[33,36] studies have been performed demonstrating coherent actions of nearest Lewis and Brønsted sites in enhanced acidic properties. Formation of some EFAL moieties upon consequent dealumination was approved via combined[37] Al TQ-MAS NMR and DFT computations.[33,36] The next logical step

dx.doi.org/10.1021/ic301279v | Inorg. Chem. XXXX, XXX, XXX−XXX

Table 6. Frequencies of Stretching (ν_{HF}, ν_{LF}) and Bending (ν_{B1}, ν_{B2}) Modes (cm^{-1}), Zero Point Energies (ZPE = $hc(\nu_{HF} + \nu_{LF} + \nu_{B1} + \nu_{B2})/2$, kcal/mol, c is velocity of light), and Heat of Adsorption for Water $\Delta U_{H2O} = E_{cell+H2O} - E_{cell} - E_{H2O}$ at the PBE and PW91 Levels in LaMOR Forms (Figure 2a–g)[a]

	1		1a	2		2a	3		3a	4	
param	H_2O	H + OH	H + OH	H_2O	H + OH	H + OH	H_2O	H + OH	H + OH	H_2O	H + OH
						PBE					
ν_{HF}	3757.1	3781.7	3778.7	3755.1	3794.1	3777.1	3737.5	3782.2	3785.9	3747,9	3785.9
ν_{LF}	3668.7	3588.4	3600.7	3668.0	3584.4	3604.0	2821.5	3191.5	3608.1	3657,1	3599.1
ν_{B1}	1616.9	978.0	1014.4	1613.1	1012.7	1023.0	1646.1	1170.9	1010.2	1616,4	1031.8
ν_{B2}	505.9	594.6	590.6	494.6	586.1	586.3	800.2	648.7	597.6	504.6	576.7
ZPE	13.65	12.78	12.84	13.62	12.83	12.85	12.87	12.57	12.87	13.62	12.86
ΔU_{H2O}[b]	31.11			32.20			36.41			33.54	
ΔU_{H2O}+ ΔZPE[c]	31.66			32.72			36.18			34.07	
						PW91					
ν_{HF}	3755.0	3791.3	3782.8	3755.0	3797.4	3783.0	3742.3	3789.1	3794.0	3736.8	3788.3
ν_{LF}	3670.8	3588.7	3589.0	3670.7	3592.0	3599.4	2706.7	3165.8	3600.4	3618.0	3601.5
ν_{B1}	1613.3	984.3	1012.2	1614.2	1015.8	1018.8	1651.3	1180.3	1010.5	1607.0	1031.3
ν_{B2}	505.5	604.0	584.4	493.4	585.3	582.9	836.0	663.8	580.9	500.7	585.0
ZPE	13.64	12.82	12.82	13.63	12.85	12.84	12.77	12.58	12.85	13.53	12.87
ΔU_{H2O}[b]	34.49			35.41			39.96			38.13	
ΔU_{H2O}+ ΔZPE[c]	35.03			35.93			37.46			38.54	

[a]The ZPE[g] of 13.10 (PBE)/13.11 (PW91) kcal/mol in the gas state corresponds to the frequencies of 3842.9, 3732.9, 1587.2 cm^{-1} at the PBE level and to the frequencies of 3848.0, 3735.9, 1586.9 cm^{-1} at the PW91 level, ΔZPE = ZPE − ZPE[g]. [b]Without ΔZPE, full balance for the ΔU_{H2O} values is shown in Table S5 (the minus sign for ΔU_{H2O} is omitted herein) [c]Experimental heat of water adsorption is 35.0 and 33.5 kcal/mol at the lowest coverage of LaY corresponding to 195 or 20 °C, respectively.[24]

is to test their possibilities for OH group stabilization and to explain high USY acidity.

As we have mentioned earlier,[3] the independence of the most intense band of acidic OH group in the MeMOR zeolite[5] on AE cation type (Me = Mg, Ca, Sr) is a logical consequence of the remote OH location relative to the AE cation, so that the acidic OH group is not influenced by the cation. All the MeMOR forms (Si/Al = 10) with the kinetic control for the proton transfer possess the same peak 3620[5] or 3616[37] cm^{-1} for any Me = Mg, Ca, Sr. Hence, as experimental evidence in favor of the thermodynamic control for proton transfer in the RE zeolites and/or the closer OH location relative to the Me cation, we would mention the dependence of the acid Si–OH–Al peak position on the cation type in LaY (3520 cm^{-1}) or CeY (3535 cm^{-1}) zeolites rather than minor variation between respective bands in the AE types (Y or MOR).[5,37] This difference of 15 cm^{-1} between the peaks in the RE forms of two neighboring La and Ce elements should be correctly compared to the smaller value for the AE forms in the Y framework with the same Si/Al = 4.7 ratio, i.e., the OH peak positions in MgY (3600 cm^{-1}) and CaY (3595 cm^{-1}) vary within experimental error[5] (5 cm^{-1}). Even for X type (Si/Al = 2.5) with higher cation concentration the acid Si–OH–Al peaks for the MgX (3595 cm^{-1}), CaX (3590 cm^{-1}), and SrX (3600 cm^{-1}) forms drift within the more narrow interval of 10 cm^{-1} than between LaY and CeY (15 cm^{-1}). This large variation of the OH band with the cation type made Bolton propose that this OH group belongs to water molecules coordinated to the RE cation type.[38] This hypothesis should be also further discussed owing to the arguments in favor of dynamic equilibrium between water and its dissociation products whose shift to the recombination is promoted by higher water concentration in NdX and NdY.[39] More detailed information about the dependence on the cation type could be yielded from the spectra in ref 7, but the highest intensities of the acid OH peaks were not marked therein.

DISCUSSION

The electrostatic nature of the dissociation in Ca- or La-forms is often addressed to explain process 1 for either AE or RE forms, while it is not however evident which electrostatic terms could provide the energy gain. First, we should deny the larger charge transfer to dissociation products than to water as the reason for their electrostatic stabilization. This question is discussed in detail in part S2 in the Supporting Information.

The second possible reason for the electrostatic type of dissociation is the stabilization of the dipolar OH particles. We can justify this "electrostatic" term if the interaction of two forming hydroxyl groups (μ_{OH} dipole of 1.6502 D per each[40]) will be stronger as compared to that of one water molecule (μ_{H2O} = 1.855 D[41]). Beginning this discussion we should stress the following: (1) Dipole–dipole interactions between forming OH groups is weak. At the shortest distance r of 5.54 Å between the centers of the OH groups in model 3 the total energy gain or loss due to the dipole–dipole interactions cannot be larger than $\mu_{OH}^2 r^{-3}$ that is 0.291 kcal/mol or 0.013 eV. For other models r increases, and this contribution can be only smaller. While comparing possible changes between the models, one has to take into account that the dipole–dipole term is pretty similar throughout the 1a, 2a, and 3a series. (2) We consider the stabilization of only one OH dipole coordinated to La after dissociation with respect to the stabilization of water dipole. As we have earlier discussed,[42,43] the field is determined by cationic positions and not by that of Al atoms. Due to drastic fall of the field with a distance the interaction energy $\boldsymbol{\mu}\mathbf{F}$, where $\mathbf{F}$ is a total field vector at the position of the molecule with dipole $\boldsymbol{\mu}$, of the second OH dipole seems to be small relative to the interaction of the OH

dx.doi.org/10.1021/ic301279v | Inorg. Chem. XXXX, XXX, XXX–XXX

group being closest to La. More positions are available for remote OH group in the periodic MOR model than in 8R so that its interaction with the La field can be much smaller in MOR. This destabilizing interaction energy of remote OH group decreases with the larger distance relative to La in 8R cluster (Figure 2e). The minor interaction of the remote OH group with La field can be easily seen in Figure 3a−g, in which the OH orientation is not aligned along the field (as happens for OH group linked to La or for second OH group in the 8R cluster model, Figure 2c) but is determined by local interactions for the bridge OH group. The small deviation of OH group from the Si−O−Al plane also approves the domination of local interactions of remote OH relative to that with La field (ion−dipole). This deviation is described by the β angle that was found to be small[27] within a series of optimized H-forms. (Despite minimal basis set applied for optimization therein, the quadrupole coupling constants of the oxygen atoms at the Si−O(H)−Al moieties were predicted at periodic Hartree−Fock/ps-21G*(Si, Al)/6−21G*(O, H) level[26] in reasonable agreement with experimental data measured later.[44]) The β angle is extremely large (37.71°) for nonstable OH in the 8R cluster in which OH tries to align relative the EF direction (Table 4). This is one of the reasons for the instability of dissociation products (Figure 2c,d). The stabilization can come from the HB formation as in the model 3 (β = 17.67°) with |O···H| = 2.00 Å (Table 5). Hence, the discussion of one OH group is more justified for the periodic approach that confirms water dissociation.

At first glance the consideration of only one OH group in the energy balance cannot provide explanation for the higher $\mu_{OH}F_{OH}$ value relative to $\mu_{H2O}F_{H2O}$ because μ_{OH} is smaller than μ_{H2O}; i.e., μ_{OH}/μ_{H2O} = 1.6502/1.855 = 0.8895. Simultaneous variation of La charge in the complexes with water or OH does not exceed 0.08 e (in both directions, i.e., larger in La−OH or La−OH_2) that cannot also provide a large additional increase of the field. However, the relative interatomic distances show shortening of La−OH distance versus La−OH_2, one from 0.375 Å in the 8R cluster to 0.437 and 0.451 Å in the models 1−4 of MOR. The La−OH shrinkage is very important because it qualitatively explains the difference between the AE and RE spectra.[5−7] The emphasized Me−O(H)/Me−OH_2 bond length difference for RE versus AE is one of the reasons for comparable intensities of O−H vibrational transitions in the La−OH and Si−OH−Al groups. Herein, this ratio I_{HF}/I_{LF} = 1 is exactly calculated for the La8R model (see the section entitled "RE Forms. Isolated Cluster DFT and MP2 Approaches"). This ratio becomes $I_{HF}/I_{LF} \ll 1$ in the AE forms due to the position of water in the lower field near bivalent Ca cation.[6,7]

The La−OH shrinkage signifies that the F_{OH} can be larger than F_{H2O} and can lead to the electrostatic stabilization of dissociated form. How large can the increase of the F_{OH} be versus F_{H2O}? Let us consider simplified representation of the field F as an effective function of the charge q of one cation

$$F = q/R^n \quad (2)$$

where R is the distance from the site to the point charge q. Using the data from Dempsey's monograph,[45] we can calibrate the n value. The EF values have been calculated for fully ionic Na- and Ca-forms of X and Y zeolites. We adopt the values for Ca forms having no data for La and then will see the trend of n variation while changing from Na to Ca in order to predict the n change going from Ca to La. The electrostatic field was evaluated[45] at the distance R from the cationic position II between R = 1 and 2.5 Å as 6.1 and 1.3 V/Å in CaX and 6.3 and 1.8 V/Å in CaY. [For comparison with experimental values given below, these EF values do not seem to be strongly overestimated varying from 6.1 V/Å (0.119 a.e.) to 1.3 V/Å (0.025 a.e.) at the distances of 1 and 2.5 Å from Ca (1 a.e. = 51.429 V/Å).]. These data lead to n = 1.687 and 1.367, respectively. According to our calculations the La−O distance is shortened from 2.481 to 2.030 Å from La−OH_2 to the La−OH case. The F_{OH}/F_{H2O} ratio via eq 2 corresponds to 1.315 and 1.403 for n = 1.367 and 1.687, respectively. Taking into account μ_{OH}/μ_{H2O} = 0.8895, this correction $\mu_{OH}F_{OH}/\mu_{H2O}F_{H2O}$ becomes 1.216 and 1.501 for the same n values. Regarding the energy gain with the periodic calculations crudely around 1 eV (Table 2), we can evaluate the $\mu_{H2O}F_{H2O}$ energy whose fraction of 0.216 or 0.501 can provide this stability of 1 eV for the (dissociation products, i.e., calculating F_{H2O} from the following equations:

$$0.216\mu_{H2O}F_{H2O} = 1 \text{ eV} \quad (3)$$

or

$$0.501\mu_{H2O}F_{H2O} = 1 \text{ eV} \quad (4)$$

Accepting μ_{H2O} = 1.855 D = 0.730 a.e. for gas state molecule,[40] we can evaluate the F_{H2O} field as 0.233 and 0.100 a.e. from eqs 3 and 4 obtained for n = 1.687 and 1.367, respectively. These electrostatic field (EF) values have to be compared with available experimental (0.055 a.e. for O_2/CaA,[46] 0.025 a.e. for CO/Mg-β,[47] 0.019 a.e. for CO/Ca-β,[47] 0.0047 a.e. for N_2/NaRbY[48]) and calculated data for mono- and bivalent cationic forms. The calculated EF values require more explanations as obtained at the exact points in the NaCaA zeolite[49] or have been averaged over the pores of MgPHI considering the part with negative value of electrostatic potential.[42] The first EF values of 0.00388 and 0.0544 a.e. relate to the sites at the distance of 3.5 Å from the center of the NaCaA zeolite toward Na and Ca, respectively, calculated ab initio with periodic Hartree−Fock method and the 6-21G* basis set.[41] The averaged EF values which span from 0.037 to 0.045 a.e. have been obtained with hybrid B3LYP and more accurate 85-11G*(Mg)/8−31G*(T)/8-411G*(O) basis set (Table 8 of ref 42).

The absolute EF values are a very interesting point as they differ between the theory[42,49] and experiment,[47] on the one hand, and as much as twice between different experimental evaluations, for example, between refs 46 and 47, on the other hand, all obtained for bivalent cations in the Linde A,[46,49] β,[47] and PHI[42] zeolites. For LaMOR both EF values (0.233 and 0.100 a.e.) are overestimated as compared to the upper experimental value 0.055 a.e. for O_2/CaA.[46] We can propose two factors which can justify the overestimated field values for La case and confirm the importance of electrostatics for reaction 1. The first factor is the exponent n value in the expression 2, the second factor is the perturbed dipole values of OH and H_2O in the cationic $La^{3+}(H_2O)$ and $La^{3+}(OH^-)$ complexes. Let us consider the first possibility to fit the n value in eq 2 which will be more probable for La forms.

On the same basis as above we can find n = 3.269 or 1.876 over the same NaII position in X or Y forms and n = 2.156 or 1.706 over the NaIII position in X or Y.[45] These values show that n decreases going from monovalent to bivalent cation. Hence, the n drops upon shifting from Ca to La resulting in smaller energy variation between La−OH and La−OH_2 cases.

dx.doi.org/10.1021/ic301279v | Inorg. Chem. XXXX, XXX, XXX−XXX

This requires larger EF values near La than those obtained above (0.233 and 0.100 a.e.). It signifies that the model calculation eq 2 can justify the "electrostatic dissociation" term due to the stronger interaction of OH dipole with La ion if the n value (2) is only slightly lower than that estimated for ionic models of CaX and CaY,[45] i.e., 1.687 and 1.367, respectively. For example, if n falls so that $\mu_{H2O}/\mu_{OH} = F_{OH}/F_{H2O}$, then no gain can be achieved owing to the electrostatic effect at the La−OH_2 (2.481 Å) and La−OH (2.030 Å) distances obtained herein. It will happen if F_{OH}/F_{H2O} is lower than μ_{H2O}/μ_{OH} = 1.855/1.6505 = 1.124. A final answer about the stabilization will be achieved, if one would calibrate the n value (2) near the La cation and evaluate the dipoles of both water and hydroxyl coordinated to La relative to the gas dipole values. The parameters of two species (charges, multipole moments) and the electrostatic energy between them connected by chemical bond like between La and OH or H_2O have a conventional character. Due to different bonding to La their (OH or H_2O) electric moments can vary with respect to the gas. This qualitative approach above is justified by a similar bonding for both OH and H_2O in the same model (cluster or periodic).

A more certain conclusion about electrostatic impact from ion-dipole term on water dissociation can be done for the CaMOR case for which we know the n values[45] and the variation of the Ca−OH distance (1.982 Å) versus Ca−OH_2 (2.306 Å) from periodic calculations (see section entitled AE Forms). The respective Ca−O bond length variation of 0.324 Å is smaller than 0.437 and 0.451 Å in different LaMOR models. Then, F_{OH}/F_{H2O} varies from 1.230 to 1.291 for n = 1.367 and 1.687, respectively. This will lead to the $\mu_{OH}F_{OH}/\mu_{H2O}F_{H2O}$ values from 1.094 to 1.148, respectively, using the same dipole values. Then at the largest ratio (1.148) and maximal experimental EF value of 0.055 a.e.,[46] according to eqs 3 and 4, the gain is 0.162 eV or 3.73 kcal/mol ($0.148 \times \mu_{H2O}F_{H2O}$ = 0.148 × 0.73 × 0.055 = 0.0059 a.e. = 0.162 eV). This electrostatic contribution seems to be not large enough to provide the stabilization competing with the other energy terms varying between Ca−H_2O and Ca−OH. In order to confirm this conclusion more information on the n value (2) is desirable on the basis of more accurate models than ionic CaX and CaY ones.[45]

In order to verify possible changes in the electrostatic terms due to the perturbations of molecular properties accepted above for the gas state we have calculated all atomic multipole moments up to hexadecapoles at all the atoms and up to the dipoles at H atoms using the GDMA 2.0 code[20] (part S3). The DMA analysis is given for the La8R and Mg(6R + 4R) models for which the heat of dissociation is known (Table S8). We have obtained that the atomic O dipole, being the main term in the molecular OH and H_2O dipoles (part S3), overcomes the gas state value in the La8R and is smaller in Mg(6R + 4R). However, the relation between the O atomic dipoles in OH (0.956 au) and in H_2O (0.782 au) even in the La8R case is 1.22 only; that cannot provide the high field values obtained above (0.233 and 0.100 au). This devaluates the possible dominate impact of the ion-dipole term for water dissociation in the RE form, and demonstrates a complex nature of the phenomenon which cannot be only reduced to electrostatic energy. Deeper orbital analysis is not however straightforward for the case. A more detailed NBO scheme is hindered owing to pseudopotential LANL2DZ (La) basis set.[50] The application of the Kitaura−Morokuma energy decomposition[51,52] is not allowed by nonconvergence of SCF procedure for the separate charged part of the cluster without for example Me cation and water components as required by the procedure.

A traditional point of view[8,9] interprets reaction 1 as a way to fully compensate the high charge of polyvalent RE cations. However, the idea of local charge compensation was questioned recently at the computational level.[53] The authors demonstrated that the periodic DFT level favored location of the charged $(Ga_2O_2)^{+2}$ species at two distant Al atoms in GaMOR relative to their close positions. This led to the thesis of nonlocal charge compensation in aluminosilicate zeolites.[53]

CONCLUSIONS

We have analyzed the Brønsted acidity of the most acid CaMOR zeolite (relative to CaY and CaZSM-5 according to their IR signals[37]) and of the LaMOR at the cluster and periodic level. We did not find any site with two Al atoms closely located near Ca cation where water dissociates. On the opposite, the products of the dissociation are stable at any site of the LaMOR zeolite at the periodic level and with the 6R + 4R or 8R cluster models. For the last model the H position in 8R can influence the stability of the products. The isolated cluster calculations with La8R (without hydrogen bonding) reproduce the close experimental intensities of high and low frequency OH bands in the La form zeolites.[6,7]

This distinction between the AE and RE forms allows justifying the idea of both thermodynamic control (due to deprotonation energy variations) and kinetic control (due to the barrier values between the attainable O-sites) for proton locations in the RE zeolites while the proton transfer in the AE forms has to be limited kinetically only. This difference correlates with the remote location of OH groups relative to the cation in AE forms so that the vibrational OH band does not depend on the AE cation type (Mg, Ca, Sr) in MOR and Y types. On the opposite, the respective peaks of acid OH groups are shifted by 15 cm^{-1} between LaY and CeY. The last variation can be interpreted as a dependence of acid hydroxyl on the cation type.

After the distributed multipole analysis scheme of Stone we have not obtained large enough dipole variation between OH and H_2O dipoles to approve the dominant role of the ion-dipole term for the stabilization of the products of H_2O dissociation with two cluster models. Required electrostatic field values have to be too large either for La, or for Ca, relative to the experimentally measured values in different zeolite forms. This shows a complex nature of dissociation phenomenon that cannot be explained by electrostatic energy only.

ASSOCIATED CONTENT

Supporting Information

Zero point energy in adsorbed state with the cluster and periodic approaches; charge transfer to adsorbed or dissociated states in cluster or periodic models; six tables and the figure of the product of water dissociation in LaMOR. Movie of the water dissociation. This material is available free of charge via the Internet at http://pubs.acs.org.

AUTHOR INFORMATION

Corresponding Author

*E-mail: rybakovy@gmail.com.

dx.doi.org/10.1021/ic301279v | Inorg. Chem. XXXX, XXX, XXX−XXX

Author Contributions

The manuscript was written through contributions of all authors. All authors have given approval to the final version of the manuscript. All authors contributed equally.

Notes

The authors declare no competing financial interest.

■ ACKNOWLEDGMENTS

The authors deeply acknowledge Professor D.P. Vercauteren for permanent help. Part of the calculations were performed on the Interuniversity Scientific Computing Facility (ISCF), for which we gratefully acknowledge the financial support from the F.R.S.-FRFC (Convention 2.4.617.07.F) and from the FUNDP. The authors are extremely grateful to Computer Complex SKIF of Lomonosov Moscow State University "Chebyshev" for computational time and to the manager of the Complex Dr. S.A. Zhumatii for the help. The authors thank RFFI for Grant 12-03-00749-a.

■ REFERENCES

(1) Breck, D.W. *Zeolite Molecular Sieves—Structure, Chemistry and Use*; J. Wiley & Sons, Inc.: New York, 1974.
(2) Shubin, A. A.; Zhidomirov, G. M.; Yakovlev, A. L.; van Santen., R. A. *J. Phys. Chem. B* **2001**, *105*, 4928−4935.
(3) Larin, A. V.; Rybakov, A. A.; Zhidomirov, G. M. *J. Phys. Chem. C* **2012**, *116*, 2399−2410.
(4) Aleksandrov, H. A.; Vayssilov, G. N.; Rösch, N. *J. Mol. Catal. A: Chem.* **2006**, *256*, 149−155.
(5) Kustov, L. M.; Borovkov, V. Yu.; Kazansky, V. B. *J. Catal.* **1981**, *72*, 149−159.
(6) Christner, L. G.; Liengme, B. V.; Hall, W. K. *Trans. Faraday Soc.* **1968**, *64*, 1679.
(7) Ward, J. W. *J. Phys. Chem.* **1968**, *72*, 4211−4223.
(8) Cheetham, A. K.; Eddyp, M. M.; Thomas, J. M. *J. Chem. Soc., Chem. Commun.* **1984**, 1337−1338.
(9) Smith, J. V.; Bennett, J. M.; Flanigen, E. M. *Nature* **1967**, *215*, 241−244.
(10) Frisch, M. J.; Trucks, G. W.; Schlegel, H. B.; Scuseria, G. E.; Robb, M. A.; Cheeseman, J. R.; Montgomery, J. A., Jr., Vreven, T.; Kudin, K. N.; Burant, J. C.; Millam, J. M.; Iyengar, S. S.; Tomasi, J.; Barone, V.; Mennucci, B.; Cossi, M.; Scalmani, G.; Rega, N.; Petersson, G. A.; Nakatsuji, H.; Hada, M.; Ehara, M.; Toyota, K.; Fukuda, R.; Hasegawa, J.; Ishida, M.; Nakajima, T.; Honda, Y.; Kitao, O.; Nakai, H.; Klene, M.; Li, X.; Knox, J. E.; Hratchian, H. P.; Cross, J.B.; Bakken, V.; Adamo, C.; Jaramillo, J.; Gomperts, R.; Stratmann, R. E.; Yazyev, O.; Austin, A. J.; Cammi, R.; Pomelli, C.; Ochterski, J. W.; Ayala, P. Y.; Morokuma, K.; Voth, G. A.; Salvador, P.; Dannenberg, J. J.; Zakrzewski, V. G.; Dapprich, S.; Daniels, A. D.; Strain, M. C.; Farkas, O.; Malick, D. K.; Rabuck, A. D.; Raghavachari, K.; Foresman, J. B.; Ortiz, J. V.; Cui, Q.; Baboul, A. G.; Clifford, S.; Cioslowski, J.; Stefanov, B. B.; Liu, G.; Liashenko, A.; Piskorz, P.; Komaromi, I.; Martin, R. L.; Fox, D. J.; Keith, T.; Al-Laham, M. A.; Peng, C. Y.; Nanayakkara, A.; Challacombe, M.; Gill, P. M. W.; Johnson, B.; Chen, W.; Wong, M. W.; Gonzalez, C.; Pople, J. A. *Gaussian 03, Revision C.02*; Gaussian, Inc.: Wallingford, CT, 2004.
(11) Frisch, M. J.; Trucks, G. W.; Schlegel, H. B.; Scuseria, G. E.; Robb, M. A.; Cheeseman, J. R.; Scalmani, G.; Barone, V.; Mennucci, B.; Petersson, G. A.; Nakatsuji, H.; Caricato, M.; Li, X.; Hratchian, H. P.; Izmaylov, A. F.; Bloino, J.; Zheng, G.; Sonnenberg, J. L.; Hada, M.; Ehara, M.; Toyota, K.; Fukuda, R.; Hasegawa, J.; Ishida, M.; Nakajima, T.; Honda, Y.; Kitao, O.; Nakai, H.; Vreven, T.; Montgomery, J. A., Jr., Peralta, J. E.; Ogliaro, F.; Bearpark, M.; Heyd, J. J.; Brothers, E.; Kudin, K. N.; Staroverov, V. N.; Kobayashi, R.; Normand, J.; Raghavachari, K.; Rendell, A.; Burant, J. C.; Iyengar, S. S.; Tomasi, J.; Cossi, M.; Rega, N.; Millam, J. M.; Klene, M.; Knox, J. E.; Cross, J. B.; Bakken, V.; Adamo, C.; Jaramillo, J.; Gomperts, R.; Stratmann, R. E.; Yazyev, O.; Austin, A. J.; Cammi, R.; Pomelli, C.; Ochterski, J. W.; Martin, R. L.; Morokuma, K.; Zakrzewski, V. G.; Voth, G. A.; Salvador, P.; Dannenberg, J. J.; Dapprich, S.; Daniels, A. D.; Farkas, Ö.; Foresman, J. B.; Ortiz, J. V.; Cioslowski, J.; Fox, D. J. *Gaussian 09, Revision A.1*; Gaussian, Inc.: Wallingford, CT, 2009.
(12) Zhidomirov, G. M.; Larin, A. V.; Trubnikov, D. N.; Vercauteren, D. P. *J. Phys. Chem. C* **2009**, *113*, 8258−8265.
(13) Larin, A. V.; Zhidomirov, G. M.; Trubnikov, D. N.; Vercauteren, D. P. *J. Comput. Chem.* **2010**, *31*, 421−430.
(14) Rybakov, A. A.; Larin, A. V.; Zhidomirov, G. M.; Trubnikov, D. N.; Vercauteren, D. P. *Comput. Theor. Chem.* **2011**, *964*, 108−115.
(15) (a) Kresse, G.; Hafner, J. *Phys. Rev. B* **1993**, *47*, 558−561. (b) Kresse, G.; Furthmüller, J. *Phys. Rev. B* **1996**, *54*, 11169−11186.
(16) Kresse, G.; Joubert, J. *Phys. Rev. B* **1999**, *59*, 1758−1775.
(17) Perdew, J. P.; Burke, K.; Ernzerhof, M. *Phys. Rev. Lett.* **1996**, *77*, 3865−3868.
(18) Perdew, J. P.; Chevary, J. A.; Vosko, S. H.; Jackson, K. A.; Pederson, M. R.; Singh, D. J.; Fiolhais, C. *Phys. Rev. B* **1992**, *46*, 6671−6687.
(19) (a) Henkelman, G.; Uberuaga, B. P.; Jónsson, H. *J. Chem. Phys.* **2000**, *113*, 9901−9904. (b) Sheppard, D.; Terrell, R.; Henkelman, G. *J. Chem. Phys.* **2008**, *128*, 134106−134115.
(20) Ugliengo, P.; Viterbo, D.; Chiari, G. *Z. Kristallogr.* **1993**, *207*, 9−23.
(21) Stone, A. J. *J. Chem. Theory Comput.* **2005**, *1*, 1128−1132.
(22) Sun, K.; Su, W.; Fan, F.; Feng, Z.; Jansen, T. A. P. J.; van Santen, R. A.; Li, C. *J. Phys. Chem. A* **2008**, *112*, 1352−1358.
(23) Larin, A. V.; Vercauteren, D. P.; Lamberti, C.; Bordiga, S.; Zecchina, A. *Phys. Chem. Chem. Phys.* **2002**, *4*, 2424−2433.
(24) Romanovsky, B. V.; Topchieva, K. V.; Stolyarova, L. V.; Alekseev, A. M. *Kinet. Katal.* **1970**, *11*, 1525−1530.
(25) Keleman, G.; Schön, G. *J. Mater. Sci.* **1992**, *27*, 6036−6040.
(26) Kalogeras, I. M.; Vassilikou-Dova, A. *Cryst. Res. Technol.* **1996**, *31*, 693−726.
(27) Larin, A. V.; Vercauteren, D. P. *Int. J. Quantum Chem.* **2001**, *82*, 182−192.
(28) Grimme, S. *J. Comput. Chem.* **2006**, *27*, 1787−1799.
(29) Zhao, Y.; Truhlar, D. G. *J. Chem. Phys.* **2006**, *125*, 194101−194118.
(30) Shannon, R. D. *Acta Crystallogr.* **1976**, *A32*, 751−767.
(31) Corma, A.; Marie, O.; Ortega, F. J. *J. Catal.* **2004**, *222*, 338−347.
(32) Mirodatos, C.; Barthomeuf, D. *J. Chem. Soc., Chem. Commun.* **1981**, *2*, 39−40.
(33) Li, S.; Zheng, A.; Su, Y.; Zhang, H.; Chen, L.; Yang, J.; Ye, C.; Deng, F. *J. Am. Chem. Soc.* **2007**, *129*, 11161−11171.
(34) Li, S.; Huang, S.; Shen, W.; Zhang, H.; Fang, H.; Zheng, A.; Liu, S. B.; Deng, F. *J. Phys. Chem. C* **2008**, *112*, 14486−14494.
(35) Yu, Z.; Li, S.; Wang, Q.; Zheng, A.; Chen, L.; Jun, X.; Deng, F. *J. Phys. Chem. C* **2011**, *115*, 22320−22327.
(36) Yu, Z.; Zheng, A.; Wang, Q.; Chen, L.; Xu, J.; Amoureux, J.-P.; Deng, F. *Angew. Chem., Int. Ed.* **2010**, *49*, 8657−8661.
(37) Xu, J.; Mojet, B. L.; Lefferts, L. *Microporous Mesoporous Mater.* **2006**, *91*, 187−195.
(38) Bolton, A. P. *J. Catal.* **1971**, *22*, 9−15.
(39) Stavitskaya, G. P.; Ryskin, Ya.I.; Zhdanov, S. P. *Russ. Chem. Bull.* **1978**, *27*, 24−48.
(40) Nelson, D. D., Jr.; Schiffman, A.; Nesbitt, D. J.; Orlando, J. J.; Burkholder, J. B. *J. Chem. Phys.* **1990**, *93*, 7003−7019.
(41) Lovas, F. J. *J. Phys. Chem. Ref. Data* **1978**, *7*, 1445−1750.
(42) Larin, A. V.; Sakodynskaya, I. K.; Trubnikov, D. N. *J. Comput. Chem.* **2008**, *29*, 2344−2358.
(43) Larin, A. V.; Trubnikov, D. N.; Vercauteren, D. P. *Int. J. Quantum Chem.* **2007**, *107*, 3137−3150.
(44) Peng, L.; Huo, H.; Liu, Y.; Grey, C. P. *J. Am. Chem. Soc.* **2007**, *129*, 335−346.
(45) Dempsey, E. *Molecular Sieves*; Society of Chemical Industry: London, 1968; p 293.
(46) Jousse, F.; Cohen de Lara, E. *J. Phys. Chem.* **1996**, *100*, 233−237.

(47) Li, P.; Xiang, Y.; Grassian, V. H.; Larsen, S. C. *J. Phys. Chem. B* **1999**, *103*, 5058−5062.
(48) Marra, G. L.; Fitch, A. N.; Zecchina, A.; Ricchiardi, G.; Salvalaggio, M.; Bordiga, S.; Lamberti, C. *J. Phys. Chem. B* **1997**, *101*, 10653−10660.
(49) White, J. C.; Nicolas, J. B.; Hess, A. C. *J. Phys. Chem. B* **1997**, *101*, 590−595.
(50) Carpenter, J. E.; Weinhold, F. *THEOCHEM* **1988**, *169*, 41−62.
(51) Morokuma, K *J. Chem. Phys.* **1971**, *55*, 1236−1244.
(52) Kitaura, K; Morokuma, K *Int. J. Quantum Chem.* **1976**, *10*, 325.
(53) Pidko, E. A.; Hensen, E. J. M.; Zhidomirov, G. M.; van Santen, R. A. *J. Catal.* **2008**, *255*, 139−143.

dx.doi.org/10.1021/ic301279v | *Inorg. Chem.* XXXX, XXX, XXX−XXX